# THE STRUCTURE OF ZERO, FAVORABLE AND ADVERSE PRESSURE GRADIENT TURBULENT BOUNDARY LAYERS

**Zambri Harun**[1]
Dept. of Mechanical Engineering
The University of Melbourne
Victoria 3010, Australia
[1]zambriharun@yahoo.com

**Jason P. Monty**[2] **& I. Marusic**[3]
Dept. of Mechanical Engineering
The University of Melbourne
Victoria 3010, Australia
[2]montyjp@unimelb.edu.au
[3]imarusic@unimelb.edu.au

## ABSTRACT

The effects of pressure gradient on an initially zero-pressure-gradient turbulent boundary layer are investigated. We consider both adverse and favourable pressure gradients at matched Reynolds number as compared with the zero pressure gradient case. The data are also acquired using matched sensor parameters so that an unambiguous comparison can be made. The results show that energy increases throughout the turbulent boundary layer as the pressure gradient increases. It is also found that the large-scale motions are much more energetic for adverse pressure gradients compared with the other cases. The outer region of the flow appears most affected by the pressure gradient in this regard. The streak spacing in the near-wall viscous region is found to be unaffected by the pressure gradients, which is in contrast to other studies in the literature.

## INTRODUCTION

Of the turbulent boundary layer flows, the canonical zero-pressure-gradient (ZPG) case, on a flat plate with constant free-stream velocity, has received the most attention. Recent reviews on these flows (Smits *et al.* 2011, Marusic *et al.* 2010, Klewicki 2010) discuss the recent findings with respect to scaling, Reynolds numbers effects, and the role of coherent structures and very-large-scale motions in these flows. It is of interest to see how these features change once the boundary layers encounter a streamwise favorable pressure gradient (FPG) or adverse pressure gradient (APG), as this is a common occurrence in many engineering systems. Pressure gradient flows have also received considerable attention (Clauser 1954, Cal *et al.* 2008, Krogstad & Skare 1995, Marusic & Perry 1995, Aubertine & Eaton 2000, and many others) but in recent times there has been renewed interest in the light of independent wall-shear stress measurements that have brought into question the universal scaling behaviour of the near-wall and logarithmic regions (Nagib *et al.* 2009, Bourassa & Thomas 2009, Monty *et al.* 2011). A recent DNS study of an adverse pressure gradient boundary layer by Lee & Sung (2009) has also raised questions as to how the coherent structures are affected - from the largest structures in the flow (Hutchins & Marusic 2007) to the near-wall sublayer streaks (Kline *et al.* 1967). Lee & Sung report that under strong adverse pressure gradients the near-wall streaks are weakened, with the spanwise spacing between the streaks becoming irregular and increasing in size to 400 viscous wall units, which is approximately four times larger than that of the ZPG flow. For FPG flows, these streak spacings have also been reported to be above the nominal ZPG value of 100 viscous wall units (Bourassa and Thomas 2009). A survey from various studies of streak spacing for different pressure gradient flows is shown in table 1. From these results, it is noted that significant effects are seen in the near-wall region (by the change in streak spacing).

However, all the studies in table 1 were performed at different Reynolds numbers. Here, $Re_\theta = \theta U_1/\nu$ is the Reynolds number based on momentum thickness $\theta$, where $U_1$ is the local free stream velocity and $\nu$ is kinematic viscosity. Recent studies in ZPG flows have demonstrated that Reynolds number effects vary even beyond Reynolds numbers traditionally considered high: The contribution from the log region to the overall turbulence production increases with Reynolds number (Marusic *et al.* 2010) and large-scale structures which inhabit the log region amplitude-modulate the near-wall region (Mathis *et al.* 2009). In an attempt to isolate any Reynolds number effects, we have designed experiments where we maintain the Reynolds number at $Re = \delta U_\tau/\nu \approx 1900$, where $\delta$ is the boundary layer thickness, and $U_\tau$ is friction velocity.

Throughout this paper, $x$, $y$ and $z$ are the streamwise, spanwise and wall-normal directions respectively, and nor-

| Workers | $Re_\theta$ | Pressure Gradient | Streak spacing, $\lambda_y^+$ |
|---|---|---|---|
| Bourassa & Thomas (2009) | 4590 | FPG, $K \approx 4.4 \times 10^{-6}$ | $> 100$ |
| Finnicium & Hanratty (1988) | - | FPG, $K \approx 2 \times 10^{-6}$ | 105-110 |
| Robinson (1991) review paper | range of $Re_\theta \leq 6000$ | ZPG | 100 |
| Adrian *et al.* (2000) | 930-6845 | ZPG | 100 |
| Skote & Henningson (2002) | 300-700 | ZPG to strong APG (separated) | 100 (ZPG) - 130 (Separated) |
| Lee & Sung J.S. (2009) | 1200-1400 | APG, $\beta = 1.68$ | 400 |

Table 1. A review of streak spacing in FPG, ZPG and APG boundary layers.

malization with inner variables ($U_\tau$ and $\nu/U_\tau$) is indicated by the superscript '+'. The non-dimensionalised pressure gradient parameter is defined as $\beta = \delta^*/\tau_o(dP/dx)$, where $\delta^*$ is displacement thickness and $\tau_o$ is wall shear stress, $P$ is static pressure. The acceleration parameter $K = \nu/{U_1}^2(dU_1/dx)$ will also be used.

## EXPERIMENTAL TECHNIQUES

The experiments were performed in an open-return blower wind tunnel. The important features of the tunnel are a settling chamber containing honeycomb and five screens followed by a contraction with area ratio of 8.9:1 which leads into an initial inlet section area of 940mm wide by 375mm height. The test section has an adjustable roof made from acrylic sheets and a length of 4.2m. The section heights are 375mm at the trip wire ($x$ = 0m), 400mm at $x$ = 3m and 550mm (for APG) at $x$ = 5m (or 270mm for FPG). The wind tunnel is divided into 4 sections, the inlet, the ZPG section, the APG (or FPG) section, and the outlet section. The pressure gradient was carefully adjusted so that the distribution of the coefficient of pressure $C_p$ was set to be within ±0.01 for all inlet velocities.

The turbulence measurements were made using hot-wire anemometry with single-wire probes. The hot-wire probes were operated in constant temperature mode using an AA Lab Systems AN-1003 anemometer for wire diameter, $\phi = 2.5\mu m$ and Melbourne University Constant Temperature Anemometer (MUCTA) for $\phi = 1.5\mu m$. The overheat ratio of 1.8 was used and the system had a frequency response of at least 50kHz. A Dantec probe support (55H20) was used. Wollaston wires are soldered to the prong tips and etched to give a platinum filament of the desired length, $l$. The non-dimensionalised sensor length, $l^+$, should be as small as possible to reduce spatial resolution problems (Hutchins et al., 2009). Here, $l^+ = lU_\tau/\nu$. For this experiment, we have chosen $l^+$=16 ± 1.

Two-point hot wire measurements were also carried out at various wall-normal locations with one sensor stationary and the other traveling in the spanwise direction. A typical set-up is shown in figure 2. In order to perform measurement with two moving sensors, a two-axis traverse was constructed. Both axes could travel in the wall-normal direction, however only one axis could move in the spanwise direction. The construction of the traverse and the modifications to the wind tunnel were made such that both axes could travel at least 1.5 times the boundary layer thickness in wall-normal direction and two times the boundary layer thickness in the spanwise direction. The axes were motorized by very fine stepper motors which allowed fine incremental movement between measurements. Practically, the facility allowed two-sensor measurement at any wall-normal and spanwise coordinate within the limits mentioned.

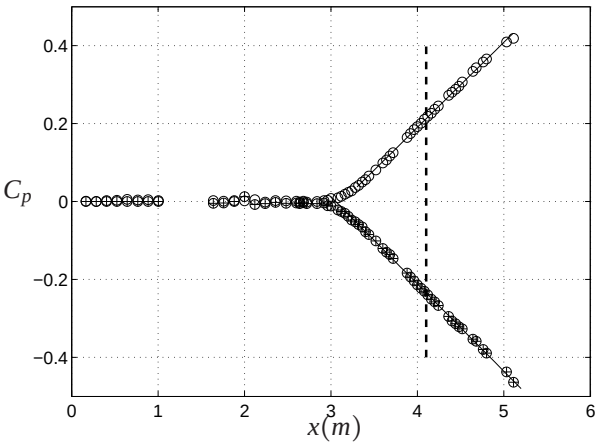


Figure 1. Coefficient of pressure $C_p$

Figure 2. Photograph of the hot-wire sensors near the wall in the two-point correlation experiments. The floor reflects the image, allowing determination of initial wall position.

Oil film interferometry (OFI), was used to independently determine the skin friction coefficient $C_f$. OFI measurements were conducted at the same location where the hot-wire anemometer measurements had been performed. 30cSt and 200cSt Dow Corning 200 Fluids were used. A Hilbert Transform (HHT) method discussed by Chauhan *et al.* (2010) was used in the analysis of OFI. Detailed descriptions of the OFI method, its background and calibration can be found in Ng *et al.* (2007).

## EXPERIMENTAL PARAMETERS

The experimental parameters are summarized in table 2. The experiments were designed so that a ZPG boundary layer was the base case and APG and FPG flow developed from

| Symbol | $U_1$ m/s | $x$ m | $Re_\tau$ | $Re_\theta$ | $\delta$ m | $\Pi$ | $\beta$ | $K$ $\times 10^{-7}$ | $\nu/U_\tau$ $\mu m$ | $d$ $\mu m$ | $l^+$ | $t^+$ | $TU_\infty/\delta$ |
|---|---|---|---|---|---|---|---|---|---|---|---|---|---|
| $\oplus$ FPG | 12.38 | 4.1 | 1930 | 3900 | 0.057 | 0.20 | -0.64 | 2.17 | 29.5 | 1.5 | 16 | 0.19 | 19600 |
| $\triangleright$ ZPG | 14.24 | 3.0 | 1830 | 5020 | 0.052 | 0.65 | ZPG | ZPG | 28.7 | 2.5 | 17 | 0.38 | 21800 |
| o APG | 11.40 | 4.1 | 1940 | 8860 | 0.078 | 1.32 | 1.77 | -1.94 | 40.7 | 2.5 | 16 | 0.19 | 21900 |

Table 2. Experimental parameters for hotwire experiments at matched $Re_\tau \approx 1900$ data. Superscript '+' is used to denote viscous scaling e.g. $U^+ = U/U_\tau$, $t^+ = tU_\tau{}^2/\nu$. $t^+ = tU_\tau{}^2/\nu$ is the non-dimensionalised sample interval, where $t = 1/f_s$, $f_s$ is sampling rate. The total length in seconds of the velocity sample at each height is given by $T$. This is non-dimensionalized in outer scaling to give boundary-layer turnover times $TU_\infty/\delta$.

there in separate cases. Figure 1 shows the $C_p$ profiles plotted against streamwise distance. It is noted that the pressure gradients are moderate, but the APG case has a similar $\beta$ value to Lee & Sung (2009). The dashed-line in this figure indicates the location at which the APG and FPG measurements were performed. The measurement stations were chosen so that the Reynolds number was nominally constant.

## RESULTS

### Mean statistics

Figure 3 shows profiles of the mean velocity and the streamwise turbulence intentities for the experiments performed at $Re_\tau \approx 1900$. Figure 3*a* shows the expected trends in mean velocity: the inner regions remains similar, while the outer region exhibits a rising wake with increased pressure gradient. The plot also provides an indication of the strength of the pressure gradients studied. The aim here is to investigate the changes from a canonical state due to pressure gradient and so mild pressure gradients have been chosen.

The turbulence intensity profiles of figure 3*b* are unique since the hot-wire sensor length (non-dimensionalised) *and* the Reynolds number has been kept constant. It is clear from this plot that there is a rise in turbulent energy (streamwise) with increased pressure gradient. Note that the turbulence intensity is scaled with the friction velocity, $U_\tau$. This scale is chosen since we are investigating variations compared to the zero pressure gradient boundary layer, where $U_\tau$ scaling is commonly employed. Although not shown here, turbulence intensity rises in the outer region even when the local freestream velocity is used as the scaling parameter. Therefore, the main conclusions of this study are not affected by choice of velocity scale.

In the following section, we examine the scales of motion that contribute to this rise in turbulence intensity.

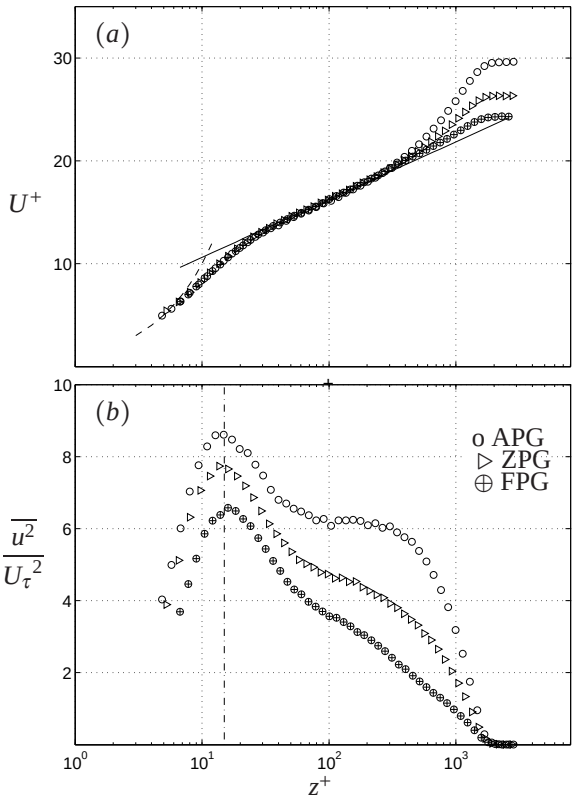


Figure 3. ZPG, APG and FPG flows at matched $Re_\tau \approx 1900$ (a) Mean velocity profiles (b) Broadband turbulence intensity profiles. For symbols, refer to table 2. Solid line for $U^+ = \kappa^{-1}\ln(z^+) + A$, $\kappa = 0.41$ and $A = 5.0$, dashed line for $U^+ = z^+$ and dashed-dot line for $z^+$=15.

### Energy spectra

Contour plots of premultiplied power spectral density are shown in figure 4, with axes indicating scaled wavelength and wall-distance. To convert from frequency to wavelength, the local mean velocity is assumed to represent the convection velocity of the turbulence. These plots give a global view of the energy distribution through the boundary layer. The area under any given vertical slice through these plots represents the turbulence intensity as shown in figure 3*b*. Therefore it is expected that there is an overall increase in energy as the pressure gradient is increased. Interestingly, the peak energy in the outer region is highlighted with symbol '■' and it appears that the outer peak in APG flows occurs at lower wavelength and greater wall-distance compared with the ZPG case (the FPG case does not exhibit a large-scale peak at this Reynolds number). It is also clear that there is significantly more energy in the outer region at large wavelengths in the APG case.

In figure 5 selected plots of the energy spectra are shown to give a clearer picture of specific energetic scales at a range of wall-distances. At the start of the logarithmic region, it is observed that the FPG flow has a higher small-scale energy content relative to the large-scales. For the ZPG case, the energy is approximately balanced between small– and large-scales, but in the APG case, the large-scales dominate. This represents a significant structural difference between the three flows and is particularly important in light of the recent studies of Mathis *et al.* (2009) who have shown an influence of

the large-scales (*centred* in the log region) through the zero pressure gradient boundary layer.

In the outer region, figure 5*d* indicates the structure of the flow is similar in all flows, with an energy peak around $\lambda = 3\delta$; the magnitude of the energy, however, increases with pressure gradient as expected from the turbulence intensity profiles.

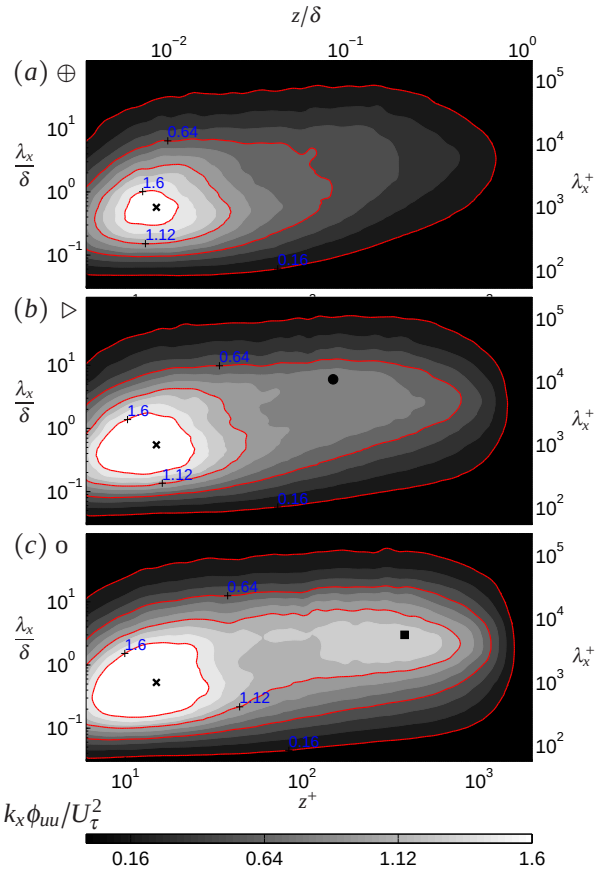


Figure 4. Pre-multiplied energy spectra of streamwise velocity fluctuation $k_x\phi_{uu}/U_\tau^2$ at constant $Re_\tau$ for different pressure gradients. Contour levels are from 0.16 to 1.6 in step of 0.16; The symbol '×' denotes the location of ($z^+ = 15$, $\lambda_x^+ = 1000$), '●' denotes the location of ($z^+ = 3.9Re_\tau^{1/2}$, $\lambda_x = 6\delta$) and '■' denotes the location of ($z/\delta = 0.2$, $\lambda_x = 3\delta$).

## Two-point streamwise velocity correlations

The two-point velocity correlation is defined and scaled as follows:

$$R_{uu}(\Delta x, \Delta y) = \frac{< u(x,y)u(x+\Delta x, y+\Delta y) >}{\sigma_u(x,y)\sigma_u(x+\Delta x, y+\Delta y)} \qquad (1)$$

where $u$ is the fluctuating velocity, $\Delta x$ and $\Delta y$ are in plane separations between the two components and $\sigma$ is the standard deviation. Figure 6 displays plots of the two-point correlations in the spanwise and streamwise directions at two wall-normal

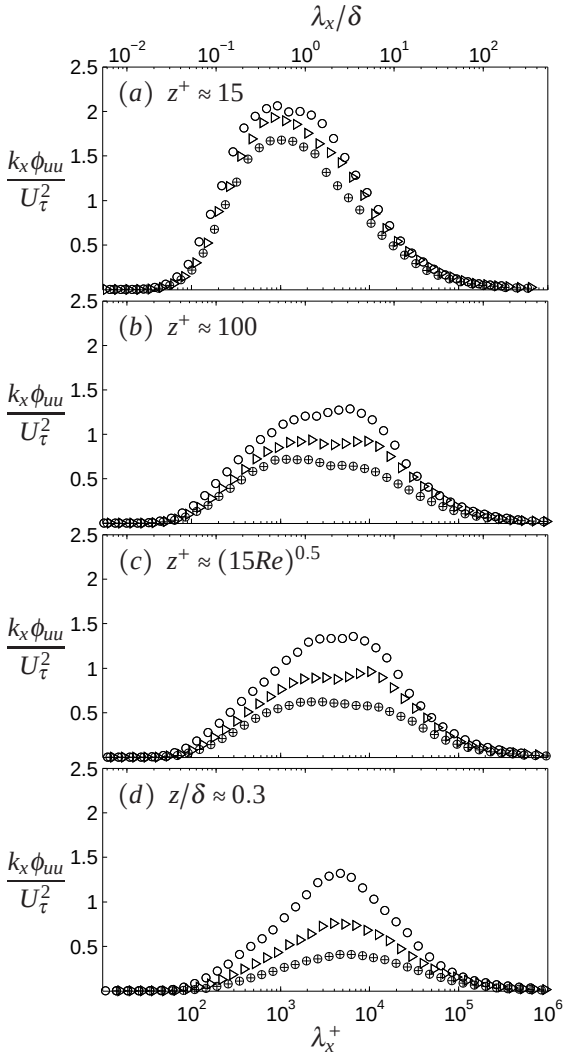


Figure 5. Pre-multiplied energy spectra of streamwise velocity $k_x\phi_{uu}/U_\tau^2$. The symbols are as in figure 3.

locations. The wall-normal locations chosen are at the near-wall peak ($z^+ \approx 15$) and in the outer region ($z \approx 0.3\delta$). In contrast to the findings of Lee & Sung (2009), there appears little evidence of any change to the near-wall cycle. The spacing between the troughs indicated in figure 6($b$) indicates that the steak spacing is invariant with pressure gradient. This obviously not in agreement with the streak spacing especially for ZPG as shown in table 1. However, these correlations contain both large- and small-scale information. To look at the small-scales independently, the original velocity fluctuations from both hotwire sensors have been filtered to remove the large-scale velocity fluctuations. The resulting correlation of the small-scale velocity fluctuations is shown in figure 7. The data presented here show that the streak spacing in the APG case is much closer to 100 wall units rather than 400 (as found by Lee & Sung). In fact it appears that the streak spacing is slightly less in the APG case.

Figures 6*c*, *d* show the correlations at $z \approx 0.3\delta$. Here we see some differences in both the streamwise and spanwise two-point correlations. Initially, it would appear that the correlation tails are shorter in the streamwise direction for the APG case compared with the other cases. Such a notable

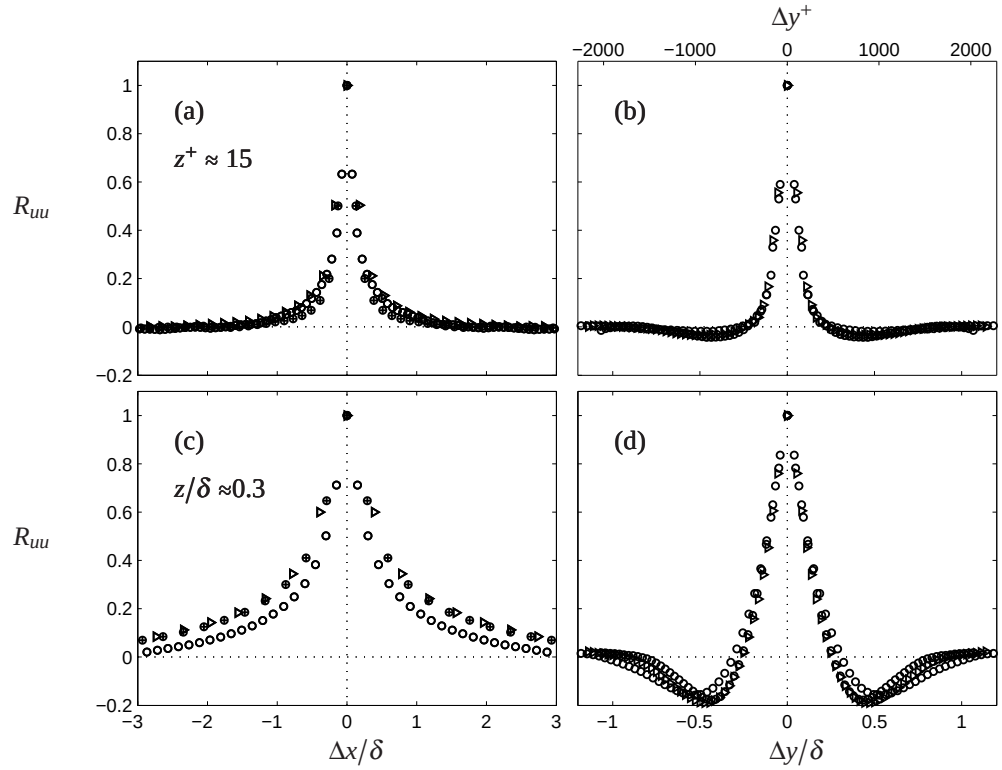


Figure 6. Streamwise (left) and spanwise (right) two-point correlation $R_{uu}$ for FPG (⊕), ZPG (▷) and APG (○) flows at $z^+ \approx 15$ (a,b) and at $z/\delta \approx 0.3$ (c,d).

shortening of length scales was not observed in the spectra shown in figure 5*d*. However, it should be noted that a convection velocity is required here to convert the temporal correlations to spatial. The convection velocity chosen is the local mean velocity. If we chose a higher (and constant) convection velocity, $0.82U_1$, for example, the correlations are much closer together as shown in figure 8. Therefore, it is difficult to discern if the characteristic length does change in pressure gradients within the uncertainty of estimating the convection velocity. The results here, do however, indicate that for the APG case the characteristic length is slightly shorter than the ZPG or FPG. In the spanwise direction, there is also a weak trend with the structures increasing slightly in width as the pressure gradient decreases. This is consistent with the idea that the FPG effect is to stretch (streamwise) and flatten the motions in the boundary layer, while the APG acts to thicken the boundary layer, causing increased structure angles and therefore reducing length scales of the individual motions.

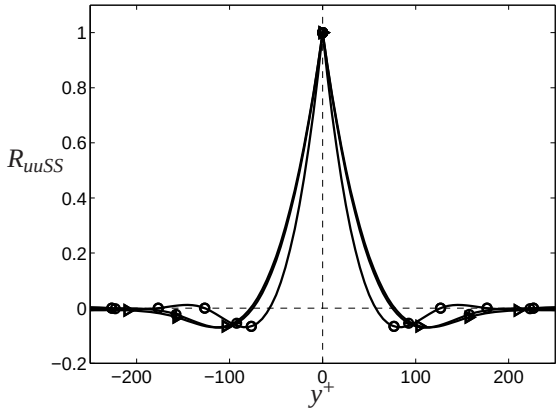


Figure 7. Correlation for small-scale velocity fluctuation, $R_{uuSS}$ in the near-wall region, $z^+ \approx 15$ for FPG (⊕), ZPG (▷) and APG (○) flows.

## CONCLUSIONS

Careful experiments with matched experimental conditions in turbulent boundary layers with zero, favorable and adverse pressure gradients have been performed at constant Reynolds number. Turbulence intensity profiles show that the streamwise kinetic energy throughout the boundary layer increases with pressure gradient. Fourier analysis indicates that there is a broadband increase of energy with pressure gradient, however, the larger scales are disproportionately energised: the APG case having the greater rise in large scale energy. Furthermore, the outer region contains much more energetic large scale structures in the APG case compared with the other cases. Previous studies Skote & Henningson (2002) and Lee & Sung (2009) have shown that these three cases have different turbulent structure in the near-wall region. However, our energy spectra and two-point correlation analyses conclude that the near-wall structures have similar streamwise and spanwise length scales. One possible reason for the discrepancy is the higher Reynolds number studied here.

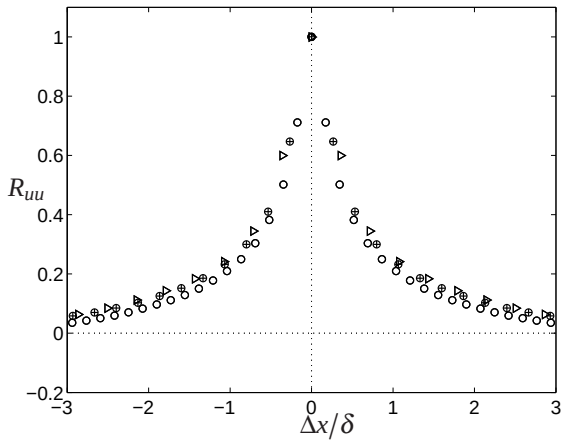


Figure 8. Figure 6*c* with $U_c = 0.82U_1$, where $U_c$ is the convection velocity.

## REFERENCES


Aubertine, C. D., Eaton, J. K., 2005,"Turbulence Development in a Non-equilibrium Turbulent Boundary Layer with Mild Adverse Pressure Gradient", J. Fluid Mech., Vol. 532, pp. 345-364.

Adrian, R.J. and Meinhart, C.D., 2000, "Vortex Organization in the Outer Region of the Turbulent Boundary Layer", J. Fluid Mech., Vol. 422, pp. 1-54.

Bourassa, C. and Thomas, F.O., 2009, "An Experimental Investigation of a Highly Accelerated Turbulent Boundary Layer", J. Fluid Mech., Vol. 634, pp. 359-404.

Cal, R.B. and Castillo, L, 2008, "Similarity Analysis of Favorable Pressure Gradient Turbulent Boundary Layers with Eventual Quasilaminarization", Physics of Fluids, Vol. 20 (105106), pp. 1-18.

Chauhan, K., Ng, H., and Marusic, I., 2010, "Empirical Mode Decomposition and Hilbert Transforms for Analysis of Oil-Film Interferograms", Meas. Sci. Technol. , Vol. 21, Issue 1054050 pp. 1-13.

Clauser, F.H., 1954, "Turbulent Boundary Layer in Adverse Pressure Gradient", J. Aero. Sci., Vol. 21, pp. 91-108.

Dixit, S.A. and Ramesh, O.N., 2010, "Large-Scale Structures in Turbulent and Reverse-Transitional Sink Flow Boundary Layers", J. Fluid Mech., Vol. 649, pp. 233-273.

Ganapathisubramani, B. Hutchins, N. Hambleton, W. T. Longmire, E. K. and Marusic, I., 2005, "Investigation of Large-Scale Coherence in a Turbulent Boundary Layer Using Two-Point Correlations", J. Fluid Mech., Vol. 524, pp. 57-80.

Harun, Z., Kulandaivelu, V., Nugroho, B., Khashehchi, M., Monty, J.P. and Marusic, I., 2010 "Large Scale Structures in an Adverse Pressure Gradient Turbulent Boundary Layer", Proceedings, 8th Int. Sym. on Engineering Turbulence Modelling and Measurements, pp. 183188.

Hutchins, N., Hambleton W.T., Marusic, I., 2005, "Inclined Cross-Stream Stereo Particle Image Velocimetry Measurements in Turbulent Boundary Layers", J. Fluid Mech., Vol. 541, 21-54.

Hutchins, N. and Marusic, I., 2007a, "Evidence of very Long Meandering Features in The Logarithmic Region of Turbulent Boundary Layers", J. Fluid Mech., Vol. 579, pp. 1-28.

Hutchins, N. and Marusic, I., 2007b, "Large-Scale Influences in Near-Wall Turbulence", Phil. Trans. R. Soc. A, Vol. 365, pp. 1-28.

Hutchins, N., Nickels, T.B., Marusic, I., and Chong, M.S., 2009, "Hot-Wire Spatial Resolution Issues in Wall-Bounded Turbulence", J. Fluid Mech., Vol. 635, pp. 103-136.

Jones M.B., Marusic, I., and Perry, A.E., 2001, "Evolution and Structure of Sink Flow Turbulent Boundary Layers", J. Fluid Mech., Vol. 422, pp. 1-27.

Kovasznay, L. S. G., Kibens, V. and Blackwelder, R. F., 1970, "Large-Scale Motion in the Intermittent Region of a Turbulent Boundary Layer", J. Fluid Mech., Vol. 41, pp. 283-325.

Krogstad, P.E., and Skåre, P.E., 1995 "Influence of a Strong Adverse Pressure Gradient on the Turbulent Structure in a Boundary Layer", Physics of Fluids, Vol. 7, Issue 8, pp. 2014-2024.

Kline, S.J. and Reynolds, W.C. and Schraub, F.A. and Runstadler, P.W., 1967, "The Structure of Turbulent Boundary Layers", J. Fluid Mech., Vol. 30, pp. 741-773.

Lee, J.H. and Sung, H.J., 2008, "Effects of an Adverse Pressure Gradient on a Turbulent Boundary Layer", Intl. J. Heat Fluid Flow, Vol. 29, pp. 568-578.

Lee, J.H. and Sung, H.J., 2009, "Structures in Turbulent Boundary Layers Subjected to Adverse Pressure Gradients", J. Fluid Mech., Vol. 639, pp. 101-131.

Marusic, I. and Perry, A.E., 1995, "A Wall-Wake Model for the Turbulence Structure of Boundary Layers. Part 2. Further Experimental Support", J. Fluid Mech., Vol. 298, pp. 389-407.

Marusic, I., Mathis, R., and Hutchins, N., 2010, "High Reynolds Number Effects in Wall Turbulence", Int. J. Heat Fluid Flow, Vol. 31, pp. 418-428.

Mathis, R., Hutchins, N. and Marusic, I., 2009, "Large-Scale Amplitude Modulation of the Small-Scale Structures in Turbulent Boundary Layers", J. Fluid Mech., Vol. 628, pp. 311-337.

Monty, J.P., Stewart, J.A., Williams, R.C. and Chong, M.S., 2007, "Large-Scale Features in Turbulent Pipe and Channel Flows", J. Fluid Mech., Vol. 589, 147-156.

Monty, J.P., N. Hutchins Ng, H.C.H., and M. S. Chong, 2009, "A Comparison of Turbulent Pipe, Channel and Boundary Layer Flows", J. Fluid Mech., Vol. 632, pp. 431-442.

Monty, J.P., Harun, Z. and Marusic, I., 2011, "A Parametric Study of Adverse Pressure Gradient Turbulent Boundary Layers", Intl. J. Heat Fluid Flow, Vol. 32, pp. 575-585.

Ng, H.C.H., Marusic, I., Monty, J.P., Hutchins, N., and M. s. Chong, 2007, "Oil Film Interferometry in High Reynolds Number Turbulent Boundary Layers", $16^{th}$ Australasian Fluid Mechanics Conference, Gold Coast, pp. 807-814.

Nagano, Y., Tsuji, T., and Houra, T., 1998, "Structure of Turbulent Boundary Layer Subjected to Adverse Pressure Gradient", Int. J. Heat Fluid Flow, 19, pp. 563-572.

Nagib, H.M. and Chauhan K.A., 2008, "Variations of von Kármán Coefficient in Canonical flows", Physics of Fluids, Vol. 20, Issue 101518, pp. 1-10.

Skote, M. and Henningson D.S., 2002, "Direct Numerical Simulation of a Separated Turbulent Boundary Layer", J. Fluid Mech., Vol. 471, pp. 107-136.